

PC²-PU: Patch Correlation and Position Correction for Effective Point Cloud Upsampling

Chen Long^{1*}, Wenxiao Zhang^{1*}, Ruihui Li², Hao Wang³, Zhen Dong^{1†}, Bisheng Yang^{1†}

¹Wuhan University, ²The Chinese University of Hong Kong, ³Rieman Lab, Huawei Technologies.
{chenlong107, dongzhenwhu, bshyang}@whu.edu.cn, {wenxxiao.zhang, wanghao4110}@gmail.com, lirh@cse.cuhk.edu.hk

Abstract

Point cloud upsampling is to densify a sparse point set acquired from 3D sensors, providing a denser representation for underlying surface. However, existing methods perform upsampling on a single patch, ignoring the coherence and relation of the entire surface, thus limiting the upsampled capability. Also, they mainly focus on a clean input, thus the performance is severely compromised when handling scenarios with extra noises. In this paper, we present a novel method for more effective point cloud upsampling, achieving a more robust and improved performance. To this end, we incorporate two thorough considerations. i) Instead of upsampling each small patch independently as previous works, we take adjacent patches as input and introduce a *Patch Correlation Unit* to explore the shape correspondence between them for effective upsampling. ii) We propose a *Position Correction Unit* to mitigate the effects of outliers and noisy points. It contains a distance-aware encoder to dynamically adjust the generated points to be close to the underlying surface. Extensive experiments demonstrate that our proposed method surpasses previous upsampling methods on both clean and noisy inputs.

Introduction

Point clouds, as a compact representation of 3D surface, provide an effective way for geometry processing. They are widely applied into many fields, such as self-driving cars (Häne et al. 2017), smart cities (Batty et al. 2012), robotics (Pomerleau, Colas, and Siegwart 2015), etc. However, raw point clouds acquired from 3D scanners are often sparse, noisy, and occluded, leading to a negative effect on the downstream works, such as point cloud segmentation and surface reconstruction. Such raw data is required to be amended and point cloud upsampling is regularly taken to densify the raw sparse input into a dense point set, thus providing a more faithful surface representation.

Thanks to the development of machine learning and deep neural networks, more and more researchers have started to use deep learning for the task of point cloud upsampling, and some good progress have been made on this task. The pioneering work (Yu et al. 2018b) uses PointNet-based (Qi et al. 2017) architecture to recover high resolution point clouds. Networks such as MPU (Yifan et al. 2019), PU-GAN (Li

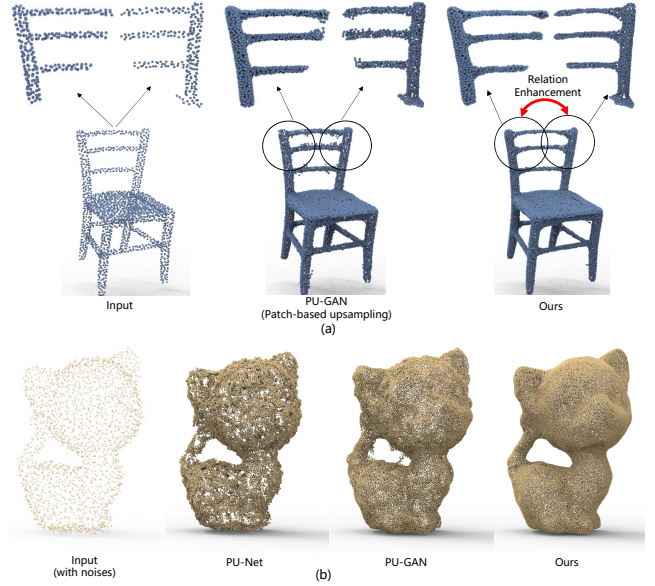


Figure 1: In the first row, existing methods only consider each individual patch when upsampling, ignoring the spatial consistency of the entire object, resulting in the loss of boundary structure of the chair. The second row shows the results of different methods when the input contains noises.

et al. 2019) and Dis-PU (Li et al. 2021) have also been gradually proposed and proved the learning-based methods to have significant advantages over the optimization-based methods (Alexa et al. 2003; Lipman et al. 2007; Huang et al. 2013).

The ultimate task of point cloud upsampling is not only to generate dense point clouds, but also to make the resulted high-resolution point clouds have high-fidelity with the true surface. The limitations of current methods are twofold. (i) Existing methods crop object into patches and upsample each patch separately, ignoring the spatial consistency and relationship between adjacent patches; (ii) Also, they focus mainly on sparse-to-dense solution with a clean input, but take less account of noises and outliers, which often occur in practical application scenarios.

To address these problems, we propose a network to han-

*These authors contributed equally.

†Corresponding Author

de the cases with stronger robustness and better performance. Our network integrates two essential modules. i) We observe that adjacent patches always have similar structures or repetitive parts, which can provide useful cues for upsampling process. Thus, we propose the Patch Correlation Unit to fully explore the relation across adjacent patches via cross transformer operation. ii) To better deal with the noises and outliers, the network should pay more attention to the relationship of relative locations between points, which reveals the interrelationship between points when generating dense points. Therefore, we propose the Position Correction Unit, using a distance-aware encoder to encode absolute and relative distance, which is fused with corresponding point features, allowing the network to adjust the generated points to be close to the input surface.

Figure 1 illustrates a visual comparison with existing methods. In Fig 1(a), we choose the chair as an example. Existing methods ignore the spatial consistency of the chair back, resulting in spurious points out of the fine boundary structure. In contrast, our network takes into account the relationship between adjacent patches, which effectively avoids these artifacts. In Fig 1(b), we show the cases when the input contains noises. Compared to current methods, our network shows its robustness. More comparison experiments show that our proposed method exceeds currently available algorithms and achieves an new SOTA.

To summarize, our main contributions are:

- We propose a novel point cloud upsampling network containing two novel modules, the Patch Correlation Unit to maintain the object’s spatial consistency and Position Correction Unit to better handle outliers and noises.
- We have designed extensive experiments on synthetic and real data sets to demonstrate the effectiveness of our network, and our network achieves the current SOTA level in both clean and noisy inputs.

Related Work

Optimization-based upsampling

In the past few decades, algorithms for point cloud upsampling have been mainly classified as optimization-based and learning-based. However, these optimization-based approaches are often not data-driven and rely heavily on a piece of prior knowledge (Lipman et al. 2007; Alexa et al. 2003; Huang et al. 2013), so they are increasingly being replaced by learning-based approaches.

Learning-based upsampling

The methods of learning-based approaches are divided into the following types: single-task and multi-task. The single-task method means that the final task is only upsampling point coordinates in the whole network structure. In contrast, the multi-task method includes multiple tasks such as normal regression, point cloud complementation, etc. They aim at getting a better model as the final goal, and each task promotes the others (Sharma et al. 2021; Zhao et al. 2020b).

PU-Net (Yu et al. 2018b) is the pioneering work on single-task upsampling, which is based on PointNet++ (Qi et al.

2017) and uses patches as the basic unit via feature expansion to achieve upsampling operation. Yu et al. proposed an edge-aware network EC-Net (Yu et al. 2018a), which focuses on consolidating the edge points. Later, Wang et al. proposed a progressive upsampling method MPU (Yifan et al. 2019), which is motivated by image super-resolution technics. Li et al. proposed a network structure called PU-GAN (Li et al. 2019) and proved that the geometric structure of sparse points is easily lost in the above algorithm. It introduces the popular GAN (Goodfellow et al. 2014) network into the upsampling task and proposes an innovative up-down-up feature expansion module. Later, Wu et al. introduced graph convolutional networks to the upsampling task of point clouds and proposed AR-GCN (Wu, Zhang, and Huang 2019) using adversarial graph loss instead of manually designed loss functions. Qian et al. proposed PU-GCN (Qian et al. 2021), arguing that the final quality of point cloud upsampling is heavily dependent on the upsampling modules and feature extractors used therein. Later, PU-GEO (Qian et al. 2020b) was proposed, which is the first upsampling algorithm that generates samples in the 2D domain and transforms them into a 3D domain by a rigorous mathematical formulation. Recently, Li et al. proposed Dis-PU (Li et al. 2021), which consists of two sub-networks that perform the tasks of generation and refinement separately instead of using a single network for upsampling. There are also some other novel research directions, such as arbitrary multiplicative point cloud upsampling (Ye et al. 2021; Qian et al. 2020a), self-supervised point cloud upsampling (Liu et al. 2020).

Existing methods mainly focus on getting dense results, but take less account of noises and outliers in real-scanned data. Therefore, they can not handle the case where the point set contains outliers and noises. In addition, existing methods follow patch-based upsampling principle, ignore the coherence and relation between the entire surface, some subtle structures are easily lost, limiting the capability of upsampling. To this end, we propose a new network containing two modules, the Patch Correlation Unit to maintain the object’s spatial consistency and Position Correction Unit to better handle outliers and noises.

Method

Overview

Figure 2 shows the overall framework of our method. We define $P = \{p_i\}_{i=1}^N$ as the low-resolution input and $Q = \{q_i\}_{i=1}^{rN}$ as the corresponding high-resolution output, where r is the upsampling rate and N is the number of input points. P_1 and P_2 denote two adjacent patch pairs. In the whole network structure, the Point Feature Extraction module follows the design of MPU (Yifan et al. 2019), the Feature Expansion Unit comes from PU-GAN, and the Coordinate Regression module is a simple MLP to regress the features to the point coordinates. In addition, to improve performance and to handle the outliers and noisy points, we propose two modules named Patch Correlation Unit and Position Correction Unit, which are detailed in the following subsections.

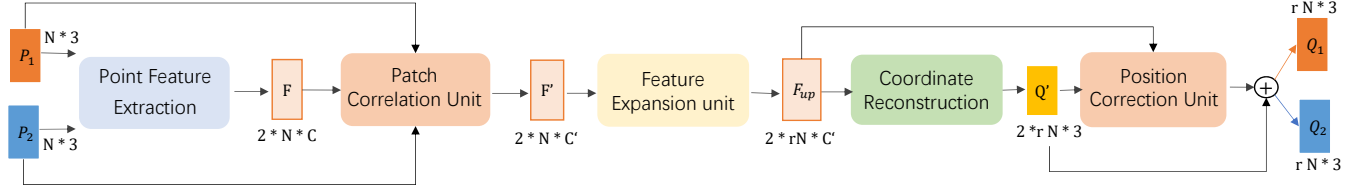


Figure 2: An illustration of our framework. Given a pair of low-resolution inputs P_1 P_2 , our network first passes them through the Point Feature Extraction module to obtain point-wise features F . Both F and P are then used as inputs to enhance the features through our Patch Correlation Unit. Then, the enhanced features F' passed through the Feature Expansion and Coordinate Reconstruction modules to obtain the coarse upsampled point cloud Q' . Finally, we use a Position Correction Unit to regress offsets to each points in Q' to get the final refined high resolution output Q .

Patch Correlation Unit

Unlike existing patch-based methods which consider each patch isolatedly, the proposed Patch Correlation Unit aims to combine the information between adjacent patches to fully explore the neighboring relations. As there are often overlaps and some similar structure implying the relations between adjacent patches, we consider this information can enhance the corresponding point features.

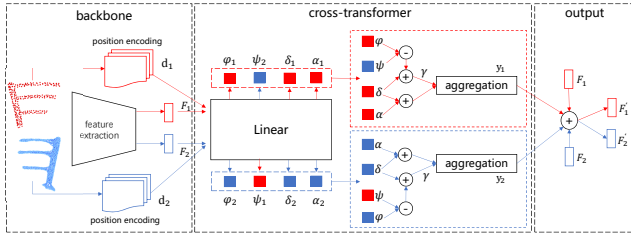


Figure 3: An illustration of Patch Correlation Unit.

Figure 3 shows the detailed design of the Patch Correlation Unit. After point-feature extraction, we get the extracted features F_1 and F_2 . Given adjacent low-resolution point clouds P_1 and P_2 with corresponding features F_1 and F_2 , we first pass them through a linear layer to reduce the size of F from C dimension to C' dimension, $C' < C$. Then the features F are fused with the position code d using the cross-transformer layer. Finally, the fused features are summed with the feature F to get F' , completing the fusion of the neighboring patch information. Inspired by (Zhao et al. 2020a), we design a cross-transformer module which is apply across adjacent patches P_1 and P_2 , as shown in Equation 1.

$$y_1^i = \sum_{\substack{F_2^j \in F_2(i) \\ F_1^j \in F_1(i)}} \gamma(\varphi(F_1^i) - \psi(F_2^j) + d_1^i) \odot (\alpha(F_1^j) + d_1^i), \quad (1)$$

where F_1 and F_2 are features of a pair of adjacent patches, F_1^i and y_1^i are the input and output of the i th point in P_1 . $F_1(i)$ is the feature set of the nearest K points in the Euclidean Space of the feature F_i at the i th point in P_1 . $F_2(i)$ is the set of features of K randomly selected points in P_2 , where d_1^i indicates the position code of the i th point in P_1 and the specific formula is described in the next section. The

symbol $\gamma, \varphi, \psi, \alpha$ denote a simple MLP layer and \odot denotes element-wise product operation.

Such a module looks for correlations between adjacent patches in feature space through the operation of a cross transformer. It makes each patch take into account the information between adjacent patches when obtaining a coarse point cloud, thus effectively maintains the spatial consistency of the overall object and improves the performance.

Position Correction unit

Existing networks such as PU-Net, PU-GAN, etc., try to generate uniformly distributed points on the object surface as possible. However, this approach is not suitable for dealing with outliers and noises. For noises, uniform distribution will result in generated point between the noises and the true surface of the point set, as shown in Figure 1 (b). Therefore, to better deal with outliers and noises, we propose another module named Position Correction Unit, which contains a position encoder that encodes the relationship of relative locations between points. Using such relative location relations enables the network to distinguish the differences between outliers and other points to adjust the position of the generated points to approach the surface, reducing the impact caused by noises and outliers. After obtaining

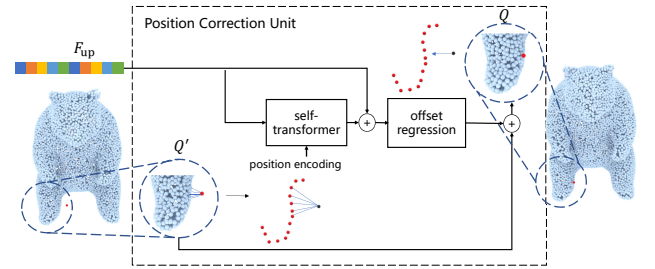


Figure 4: An illustration of Position Correction Unit

the initial upsampled point cloud Q' , we correct the coarse point cloud via our Position Correction Unit. Our position correction module is shown in Figure 4. First, we take the expanded features F_{up} and the rough point cloud Q' as input and pass Q' through a position encoder to obtain a distance encoding d . F_{up} and d are then fed into a self-transformer module to get enhanced features. Next, we regress an offset

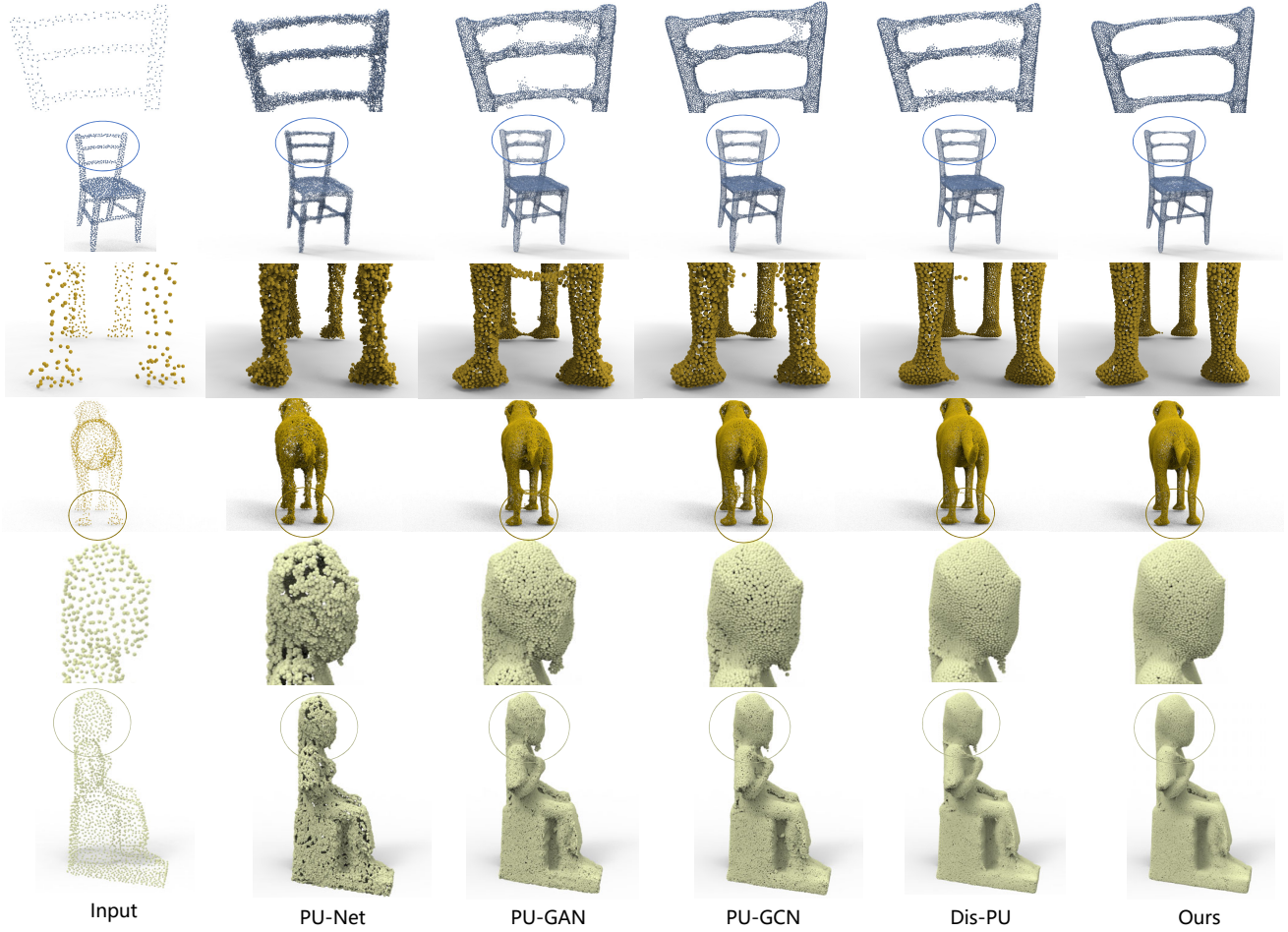


Figure 5: Visual comparisons between our method and state-of-arts. We performed visual comparison experiments on the benchmark dataset using 16X upsampling, where 16X indicates upsampling multipliers $r = 16$.

through the enhanced features to correct point position using a simple MLP, which will be added to Q' to obtain the final high-resolution output Q .

The network architecture of self-transformer can be expressed by the following Equation 2.

$$y^i = \sum_{F^j \in F(i)} \gamma(\varphi(F^i) - \varphi(F^j) + d^i) \odot (\alpha(F^j) + d^i), \quad (2)$$

where $F(i)$ is the set of features of the nearest K points in Euclidean space for the i th point in Q' .

The most important design in this whole module is the position encoder. Inspired by RAND-LA (Hu et al. 2020), we have introduced a position encoder to the task of sampling on point clouds, formulated by

$$d^i = d^i(1) \oplus \dots \oplus d^i(k) \quad (3)$$

$$d^i(k) = MLP(p_i \oplus p_i^k \oplus (p_i - p_i^k) \oplus \|p_i - p_i^k\|), \quad (4)$$

where d^i denotes the position code of the i th point, which consists of a series of K one-dimensional vectors, and $d^i(k)$ is the k th feature channel of d^i . p_i is the coordinate of

the point, p_i^k is the k th neighboring point of point i in the Euclidean Space. \oplus is for the concatenation operator, and $\|p_i - p_i^k\|$ is for the Euclidean distance.

We use a position encoder to obtain a position code d , which contains the relative location relations, especially the L1 distance and L2 distance of each point to its nearest K neighboring points. Such a position encoder preserves the relative relationship between points, and it is also distance-sensitive so that the network can clearly distinguish the presence of noises and outliers. In addition, the relationship of relative locations between points can also be used as cues to adjust the weight of each adjacent point on the generated points' position, which can mitigate the impact of outliers and noises on the upsampling task. We also use this encoder in our Patch Correlation Unit to reduce the effect of noises and outliers.

Loss function

Reconstruction loss In order to make the final generated points more distributed over the object surface, we used the Earth Mover's Distance(EMD) (Fan, Su, and Guibas 2017)

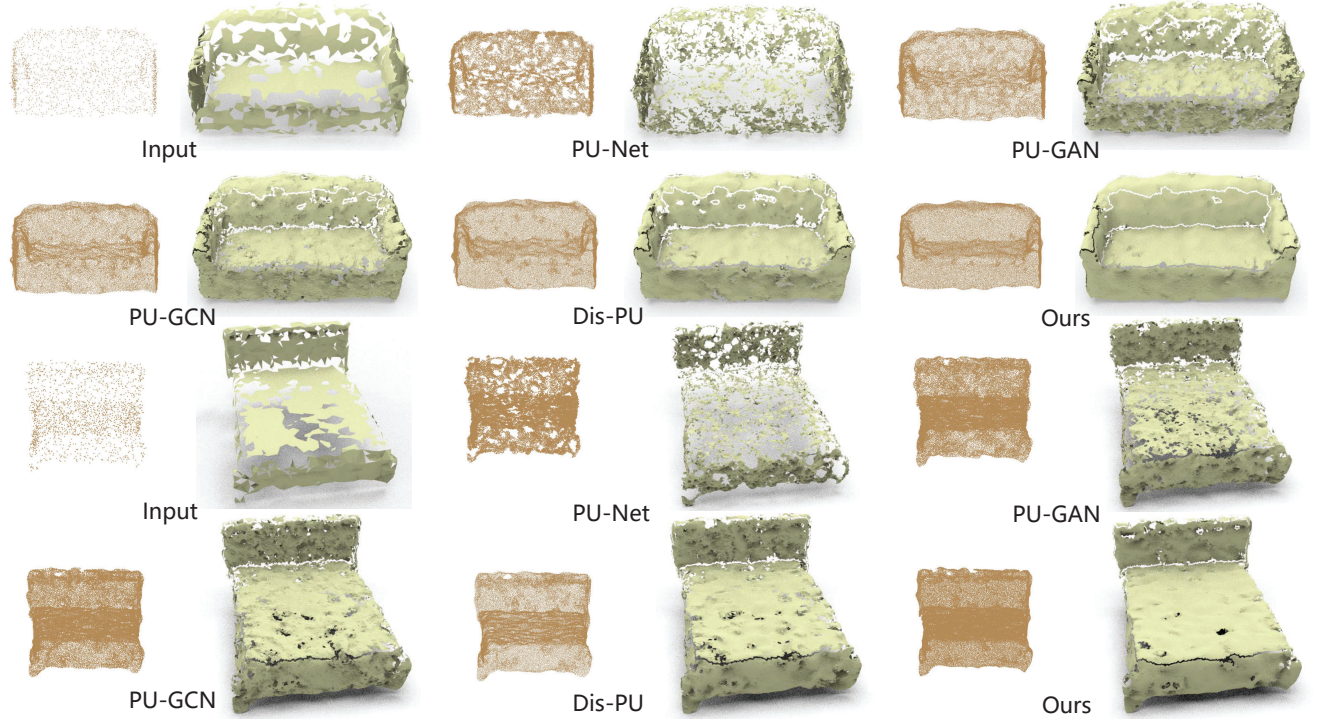


Figure 6: Real-scanned data upsampling test visual comparison. We compared the visual effects of the reconstructed model using 16X upsampling on the real dataset. The output of our network is significantly more complete in the presence of high noises and has a smoother surface. 16X indicates upsampling multipliers $r = 16$.

as the reconstruction loss function.

$$L_{rec} = L_{EMD}(Q', \hat{Q}) + \lambda L_{EMD}(Q, \hat{Q}) \quad (5)$$

$$L_{EMD}(Q_1, Q_2) = \min_{\phi: Q_1 \rightarrow Q_2} \sum_{q_i \in Q_1} \|q_i - \phi(q_i)\|_2, \quad (6)$$

where: $\phi : Q_1 \rightarrow Q_2$ is the bijection mapping. Q' is the coarse point cloud obtained after the coordinate regression, and \hat{Q} is the ground truth corresponding to the low-resolution input. The λ changes as the training rounds increases, to wait for the coarse point cloud generation to be stabilised.

Regularization loss The regularisation loss is used to prevent network overfitting, and here we have chosen the L2 regularisation loss as shown In Equation 7. Where θ indicates the parameters in our network.

$$L_{reg} = \|\theta\|_2. \quad (7)$$

Compound loss Overall, our loss function consists of two main components: reconstruction loss and regularization loss. The specific loss function, as shown in Equation 8.

$$L_{loss} = \lambda_{rec} L_{rec} + \lambda_{reg} L_{reg}, \quad (8)$$

Here λ_{rec} , λ_{reg} , are the corresponding weights given during the network training, and we will explain the settings of each hyperparameter in detail, in the next section.

Experiments

Experimental Settings

Datasets In our experiments, we include both real and synthetic datasets.

For training, we use 90 synthetic objects from the training sets provided by PU-GAN (Li et al. 2019). For each training object, we use the same sampling setting as PU-Net with a sample radius of 0.5 and randomly select 100 patch pairs, for a total of 18,000 training pairs. From these selected patches, we sample N points as our training input and rN points as our ground truth \hat{Q} using Poisson sampling. This way of creating our training dataset follows the PU-GAN (Li et al. 2019), and our training strategy is consistent with the current state-of-the-art Dis-PU (Li et al. 2021).

We test our network on both synthetic and real datasets. For synthetic datasets, we use 27 test objects provided by PU-GAN (Li et al. 2019). In order to verify the advanced performance of our network in handling noises, we use the same experimental setting as point cloud denoising network (Luo and Hu 2020), using the blensor (Gschwandtner et al. 2011) to simulate real scan data. For the real datasets, we use ScanObjectNN (Uy et al. 2019), which contains 2902 point cloud objects in 15 categories; each object has 2048 points.

Adjacent patch selection Unlike existing patch-based approaches, the input of our network is a pair of adjacent patches. For training, we randomly select 100 pairs of patches for each object and ensure that they have a suit-

able overlap to construct the training set as input. To select patches during testing, we adopt a patch selection strategy based on density clustering (Ester et al. 1996), which is detailed in the supplementary materials.

Evaluation metrics We use three commonly-used metrics: Chamfer distance(CD), Hausdorff distance (HD), and Point-to-surface distance (P2F). The smaller these metrics are, the more effective the algorithm is.

Comparison Methods To demonstrate the effectiveness of our network, we compare it with several state-of-the-art point cloud upsampling networks, including PU-Net (Yu et al. 2018b), PU-GAN (Li et al. 2019), Dis-PU (Li et al. 2021), and PU-GCN (Qian et al. 2021). We use their open-source model for testing on the same test sets.

Implementation details In experiments, we set the number of input points $N = 256$. We train our network with a batch size of 20 for 100 epochs on the TensorFlow platform. For each patch, we apply random scaling, rotation, and point perturbation to avoid overfitting. The Adam optimizer is used with the learning rate of 0.001, which is linearly decreased by a decay rate of 0.7 per 20 epochs until 10^{-6} . We set the corresponding hyperparameters of the loss function $\lambda_{rec}, \lambda_{rep}$ to 100, 1.0, respectively.

Results on Synthetic Dataset

We tested our network on the benchmark dataset provided by PU-GAN. We did not add noises and outliers to this dataset, but only sampled from the model surface using Poisson sampling to obtain this dataset. The quantitative results with other advanced networks are shown in Table 1. We can see that our network achieves a large lead in CD and HD at larger upsampling multiples. Figure 5 shows the visual comparison on the benchmark dataset. Compared with other networks, our network maintains spatial consistency after upsampling, which effectively improves the upsampling performance.

Table 1: Quantitative comparisons between our method and state-of-the-arts. The reported results are multiplied by 10^{-3} . 4X and 16X indicate upsampling multipliers $r = 4$, $r = 16$. AVG denotes the average of P2F and STD denotes the standard of P2F.

method	4X				16X			
	CD	HD	AVG	STD	CD	HD	AVG	STD
PU-Net	0.6487	5.9164	4.8238	4.3086	0.2781	3.8977	5.9453	5.0033
PU-GAN	0.2647	4.6872	1.9493	3.6153	0.2023	6.1641	2.5755	4.5649
PU-GCN	0.2630	2.8682	2.4641	3.4015	0.1515	3.9039	2.6368	4.0098
Dis-PU	0.2576	4.6713	2.0104	3.1655	0.1417	6.1985	2.2527	3.7657
Ours	0.2509	3.0418	2.2368	3.0878	0.1182	3.6507	2.4381	3.3865

Results on real-scanned data

We also conducted corresponding comparative experiments on the real dataset ScanobjectNN (Uy et al. 2019). As there is no ground truth, we only performed a visual comparison. We use the BallPivoting (Bernardini et al. 1999) algorithm to

reconstruct the result after upsampling. Figure 6 shows the visual comparison results. Compared with other networks, our network can preserve the underlying structure of the object to a certain extent so that the generated points are generated on the surface of the object as much as possible, such as the sofa back in Figure 6. Our results are smoother, without significant jitter, and with more fidelity in the overall structure. These experiments show that our network is still effective in maintaining the spatial consistency of the objects and improving the effectiveness of the network when applied to real scenarios.

Robustness Test

Noises Robust Test To demonstrate the effectiveness of our network in handling noises, we were inspired by a point cloud denoising network (Luo and Hu 2020) and designed the following experiments. First, we use the benchmark

Table 2: Noises Robust Test with Gaussian noises. We add Gaussian noises at 0.5%, 1.0%, and 2.0% levels, and use CD as the evaluation metric multiplied by 10^{-3} . 4X and 16X indicate upsampling multipliers $r = 4$, $r = 16$.

method	4X				16X			
	0.0%	0.5%	1.0%	2.0%	0.0%	0.5%	1.0%	2.0%
PU-Net	0.6487	0.5638	0.8582	1.3047	0.2781	0.3831	0.5048	0.8334
PU-GAN	0.2647	0.3379	0.5102	0.9283	0.2023	0.2672	0.3935	0.7364
PU-GCN	0.2630	0.3014	0.4269	0.8302	0.1515	0.1937	0.3229	0.6777
Dis-PU	0.2576	0.2830	0.4244	0.8410	0.1417	0.1748	0.3453	0.6904
Ours	0.2509	0.2792	0.3713	0.7380	0.1182	0.1422	0.2184	0.5486

dataset provided by PU-GAN and add different levels of Gaussian noises to the normalized objects at each object. We add 0.5%, 1.0%, and 2.0% noises, respectively, with the corresponding quantitative evaluation shown in Table 2. We can clearly see that our network shows its advantages in handling noises, and the gap between ours and other networks increases as the noises level increases. Figure 7 shows our visual comparison contrast, and the color of the dots in the figure represents the CD to the ground truth. Compared to other networks, when the noises increase significantly, we retain the object’s structure better.

Table 3: Noises Robust Test with realistic LiDAR noises simulated by blensor. We set noises at 0.5%, 1.0%, and 2.0% levels, and use CD as the evaluation metric in units of 10^{-3} . 4X and 16X indicate upsampling multipliers $r = 4$, $r = 16$.

method	4X			16X		
	0.5%	1.0%	2.0%	0.5%	1.0%	2.0%
PU-Net	0.7122	0.9388	2.0315	0.3631	0.5197	1.2855
PU-GAN	0.3587	0.6812	1.6510	0.2292	0.5078	1.4140
PU-GCN	0.3279	0.5505	1.6049	0.1655	0.3966	1.4184
Dis-PU	0.3114	0.5804	1.5874	0.1555	0.4212	1.3702
Ours	0.2854	0.4606	1.4601	0.1110	0.2643	1.1836

Besides, we randomly selected ten objects as models from the benchmark dataset provided by PU-GAN and simulate the scanning scenario using the blensor (Gschwandtner et al. 2011) plugin. Compared to directly adding Gaussian noises,

Table 4: Comparison of quantitative effects of Outliers Robust Test by using our method and state-of-the-arts. The reported results are multiplied by 10^{-3} . 4X and 16X indicate upsampling multipliers $r = 4, r = 16$ and S indicate the number of outliers.

method	S = 5								S = 10							
	4X				16X				4X				16X			
	CD	HD	AVG	STD	CD	HD	AVG	STD	CD	HD	AVG	STD	CD	HD	AVG	STD
PU-Net	0.6297	19.3565	6.4308	6.0577	0.3833	19.0181	7.1571	6.3322	0.6473	27.0540	6.5187	6.6003	0.4119	25.4899	7.2120	6.6778
PU-GAN	0.3833	17.9592	5.1006	6.3723	0.3101	18.8133	5.6296	7.1695	0.3712	24.7249	5.2338	7.3431	0.3243	24.8210	5.7635	7.9784
PU-GCN	0.3523	17.9953	3.9716	5.7602	0.2444	18.4438	4.0470	6.3729	0.3448	24.7851	4.0951	6.6463	0.2571	25.3306	4.2002	7.1670
Dis-PU	0.3329	17.4026	3.5016	5.5828	0.2291	17.9033	3.6460	6.2246	0.3349	24.9900	3.6192	6.4038	0.2402	26.1895	3.7871	6.9199
Ours	0.3177	15.2216	3.3546	4.8534	0.1827	14.9420	3.3860	4.9344	0.3039	22.0500	3.4483	5.5185	0.1598	21.1442	3.4646	5.3166

this simulation of realistic scanning method can produce more realistic point clouds and noises. We show the quantitative results in Table 3. It can be seen that our network still has a significant improvement over the existing networks when faced with realistic noises.

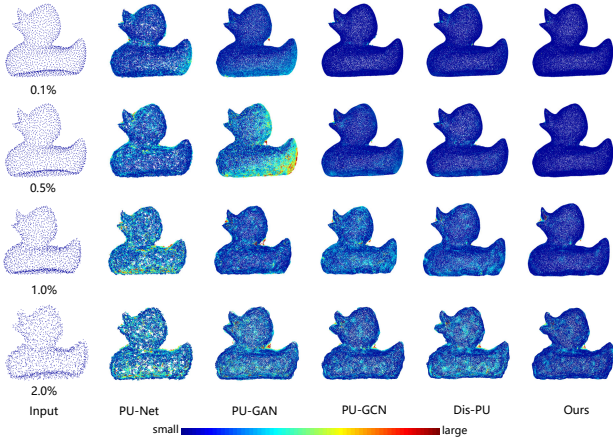


Figure 7: Noises Robust Test with Gaussian noises visual comparison. We use different levels of Gaussian noises to compare our visual effect with other networks. We use color to indicate the CD, and the smaller the CD, the better the result.

Outliers Robust Test For Outliers Robust Test, we normalized each object’s coordinates to $[0, 1]$ in the dataset, randomly selected S points and added a random vector in the range of $[-0.15, 0.15]$ to these S points as outliers. The corresponding quantitative evaluation results are shown in Table 4.

We can see that our network has significant improvement in the CD, HD and the P2F metrics compared to the original network with outliers, especially when the upsampling multiplier becomes larger.

To further demonstrate the robustness of our network, we have conducted many other experiments, such as comparing our network with existing denoising networks and more visual comparison experiments. Details are included in the supplementary material.

Ablation Study

In order to demonstrate the effectiveness of each component proposed in our network, we performed the corresponding ablation experiments by removing each component in the following cases. (I) Removal of position encoder module. (II) Removal of the Position Correction unit. (III) Removal of the Patch Correlation Unit. The experimental results are shown in the table 5.

Table 5: Ablation study. For Synthetic Dataset Test, we used 4X and 16X upsampling in benchmark datasets, which provided by PU-GAN. 4X and 16X indicate upsampling multipliers $r = 4, r = 16$. For Noises Robust Test, we set the upsampling ratio $r = 4$ and add Gaussian noises. We using CD as a quantitative evaluation metric multiplied by 10^{-3} .

model	Synthetic Dataset Test		Noises Robust Test		
	4X	16X	0.5%	1.0%	2.0%
I	0.2619	0.1313	0.2842	0.3864	0.7588
II	0.2627	0.1320	0.2856	0.3962	0.7971
III	0.2984	0.1600	0.3225	0.4371	0.8076
full model	0.2509	0.1182	0.2792	0.3713	0.7380

i) Synthetic Dataset Test. Compared to the full model, all models show a significant decline in quantitative metrics. In addition, the removal of the Patch Correlation Unit has the most severe impact on the network compared to the other cases. ii) Noises Robust Test. We tested the robustness of all the models under different levels of Gaussian noises, and we observe that each component improves the robustness of the network to some extent.

Conclusion

Existing point cloud upsampling methods focus mainly on obtaining dense results, but take less account of noises and outliers, which often occur in practical application scenarios. Meanwhile, most of these methods follow patch-based upsampling, ignoring the coherence and relation of the entire surface, thus limiting the upsampling effectiveness. To this end, we propose a new network, combining the information of adjacent patches and the relative location relations between points to improve performance and mitigate the effects of noisy points and outliers. Extensive comparative experiments show that our proposed network structure exceeds currently available algorithms to the level of current SOTA.

References

- Alexa, M.; Behr, J.; Cohen-Or, D.; Fleishman, S.; Levin, D.; and Silva, C. T. 2003. Computing and rendering point set surfaces. *IEEE Transactions on visualization and computer graphics*, 9(1): 3–15.
- Batty, M.; Axhausen, K. W.; Giannotti, F.; Pozdnoukhov, A.; Bazzani, A.; Wachowicz, M.; Ouzounis, G.; and Portugali, Y. 2012. Smart cities of the future. *The European Physical Journal Special Topics*, 214(1): 481–518.
- Bernardini, F.; Mittleman, J.; Rushmeier, H.; Silva, C.; and Taubin, G. 1999. The ball-pivoting algorithm for surface reconstruction. *IEEE transactions on visualization and computer graphics*, 5(4): 349–359.
- Chang, A. X.; Funkhouser, T.; Guibas, L.; Hanrahan, P.; Huang, Q.; Li, Z.; Savarese, S.; Savva, M.; Song, S.; Su, H.; et al. 2015. Shapenet: An information-rich 3d model repository. *arXiv preprint arXiv:1512.03012*.
- Ester, M.; Kriegel, H.-P.; Sander, J.; Xu, X.; et al. 1996. A density-based algorithm for discovering clusters in large spatial databases with noise. In *kdd*, volume 96, 226–231.
- Fan, H.; Su, H.; and Guibas, L. J. 2017. A point set generation network for 3d object reconstruction from a single image. In *Proceedings of the IEEE conference on computer vision and pattern recognition*, 605–613.
- Goodfellow, I.; Pouget-Abadie, J.; Mirza, M.; Xu, B.; Warde-Farley, D.; Ozair, S.; Courville, A.; and Bengio, Y. 2014. Generative adversarial nets. *Advances in neural information processing systems*, 27.
- Gschwandtner, M.; Kwitt, R.; Uhl, A.; and Pree, W. 2011. BlenSor: Blender sensor simulation toolbox. In *International Symposium on Visual Computing*, 199–208. Springer.
- Häne, C.; Heng, L.; Lee, G. H.; Fraundorfer, F.; Furgale, P.; Sattler, T.; and Pollefeys, M. 2017. 3D visual perception for self-driving cars using a multi-camera system: Calibration, mapping, localization, and obstacle detection. *Image and Vision Computing*, 68: 14–27.
- Hu, Q.; Yang, B.; Xie, L.; Rosa, S.; Guo, Y.; Wang, Z.; Trigoni, N.; and Markham, A. 2020. Randla-net: Efficient semantic segmentation of large-scale point clouds. In *Proceedings of the IEEE/CVF Conference on Computer Vision and Pattern Recognition*, 11108–11117.
- Huang, H.; Wu, S.; Gong, M.; Cohen-Or, D.; Ascher, U.; and Zhang, H. 2013. Edge-aware point set resampling. *ACM transactions on graphics (TOG)*, 32(1): 1–12.
- Li, R.; Li, X.; Fu, C.-W.; Cohen-Or, D.; and Heng, P.-A. 2019. PU-GAN: a Point Cloud Upsampling Adversarial Network. In *IEEE International Conference on Computer Vision (ICCV)*.
- Li, R.; Li, X.; Heng, P.-A.; and Fu, C.-W. 2021. Point Cloud Upsampling via Disentangled Refinement. In *Proceedings of the IEEE Conference on Computer Vision and Pattern Recognition (CVPR)*.
- Lipman, Y.; Cohen-Or, D.; Levin, D.; and Tal-Ezer, H. 2007. Parameterization-free projection for geometry reconstruction. *ACM Transactions on Graphics (TOG)*, 26(3): 22–es.
- Liu, X.; Liu, X.; Han, Z.; and Liu, Y.-S. 2020. SPU-Net: Self-Supervised Point Cloud Upsampling by Coarse-to-Fine Reconstruction with Self-Projection Optimization. *arXiv preprint arXiv:2012.04439*.
- Luo, S.; and Hu, W. 2020. Differentiable Manifold Reconstruction for Point Cloud Denoising. In *Proceedings of the 28th ACM International Conference on Multimedia*.
- Pomerleau, F.; Colas, F.; and Siegwart, R. 2015. A review of point cloud registration algorithms for mobile robotics. *Foundations and Trends in Robotics*, 4(1): 1–104.
- Qi, C. R.; Yi, L.; Su, H.; and Guibas, L. J. 2017. Pointnet++: Deep hierarchical feature learning on point sets in a metric space. *arXiv preprint arXiv:1706.02413*.
- Qian, G.; Abualshour, A.; Li, G.; Thabet, A.; and Ghanem, B. 2021. Pu-gcn: Point cloud upsampling using graph convolutional networks. In *Proceedings of the IEEE/CVF Conference on Computer Vision and Pattern Recognition*, 11683–11692.
- Qian, Y.; Hou, J.; Kwong, S.; and He, Y. 2020a. Deep Magnification-Arbitrary Upsampling over 3D Point Clouds. *arXiv preprint arXiv:2011.12745*.
- Qian, Y.; Hou, J.; Kwong, S.; and He, Y. 2020b. Pugeonet: A geometry-centric network for 3D point cloud upsampling. In *European Conference on Computer Vision*, 752–769. Springer.
- Sharma, R.; Schwandt, T.; Kunert, C.; Urban, S.; and Broll, W. 2021. Point Cloud Upsampling and Normal Estimation using Deep Learning for Robust Surface Reconstruction. *arXiv preprint arXiv:2102.13391*.
- Uy, M. A.; Pham, Q.-H.; Hua, B.-S.; Nguyen, D. T.; and Yeung, S.-K. 2019. Revisiting Point Cloud Classification: A New Benchmark Dataset and Classification Model on Real-World Data. In *International Conference on Computer Vision (ICCV)*.
- Wu, H.; Zhang, J.; and Huang, K. 2019. Point cloud super resolution with adversarial residual graph networks. *arXiv preprint arXiv:1908.02111*.
- Ye, S.; Chen, D.; Han, S.; Wan, Z.; and Liao, J. 2021. Meta-PU: An Arbitrary-Scale Upsampling Network for Point Cloud. *IEEE Transactions on Visualization and Computer Graphics*.
- Yifan, W.; Wu, S.; Huang, H.; Cohen-Or, D.; and Sorkine-Hornung, O. 2019. Patch-based progressive 3d point set upsampling. In *Proceedings of the IEEE/CVF Conference on Computer Vision and Pattern Recognition*, 5958–5967.
- Yu, L.; Li, X.; Fu, C.-W.; Cohen-Or, D.; and Heng, P.-A. 2018a. Ec-net: an edge-aware point set consolidation network. In *Proceedings of the European Conference on Computer Vision (ECCV)*, 386–402.
- Yu, L.; Li, X.; Fu, C.-W.; Cohen-Or, D.; and Heng, P.-A. 2018b. Pu-net: Point cloud upsampling network. In *Proceedings of the IEEE Conference on Computer Vision and Pattern Recognition*, 2790–2799.
- Zhao, H.; Jiang, L.; Jia, J.; Torr, P.; and Koltun, V. 2020a. Point transformer. *arXiv preprint arXiv:2012.09164*.

Zhao, Y.; Xie, J.; Qian, J.; and Yang, J. 2020b. PUI-Net: A Point Cloud Upsampling and Inpainting Network. In *Chinese Conference on Pattern Recognition and Computer Vision (PRCV)*, 328–340. Springer.

APPENDIX

Density Clustering Based Patch Selection

We detail our adjacent patch selection algorithm based on density clustering in Algorithm 1. We use density clustering because we believe that the more categories in the overlap, the more complex the structure of the place represents, and there may also be outliers and noisy points that require information enhancement from neighboring patches. In addition, it is worth noting that when there are no adjacent patches, the patches can be copied twice as input, which can also work accordingly.

Algorithm 1: Adjacent patch pair selection method

Input: low-resolution patch sets $PS = \{P_1, P_2, \dots, P_M\}$

Output: Pairs of patch sets $PPS = \{(P_1, P_1^{opt}), \dots, (P_M, P_M^{opt})\}$

```

1: for  $P_m$  in  $PS$  do
2:   Select the  $K$  closest patches to  $P_m$  based on distance
      $PN = \{P_m^1, P_m^2, \dots, P_m^K\}, PN \in PS$ 
3:   Get overlapping area between  $P_m$  and its neighboring
     patches.
4:    $OA = \{P_m \cap P_m^1, \dots, P_m \cap P_m^K\}$ 
5:   for  $OA_k$  in  $OA$  do
6:     Use the density clustering algorithm (Ester et al.
       1996) to cluster  $OA_k$  and get the number of clusters
        $C_k$ .
7:   end for
8:    $opt = \operatorname{argmax}(C_k), k \in \{1, 2, \dots, K\}$ .
9:   Push  $(P_m, P_m^{opt})$  to  $PPS$ 
10: end for

```

Comparison with point cloud denoising network

We use a combination of denoised and upsampled networks to compare with our network to demonstrate the superiority of our network. We use DMRDenoise (Luo and Hu 2020) as the point cloud denoising network, first use the denoising network to denoise the dataset with added Gaussian noises, and then use PU-Net, PU-GAN, etc network for upsampling before comparing the corresponding results with our network. The corresponding quantitative evaluation results are shown in Table 6.

Our network has a clear advantage over this approach. This is due to the fact that most existing point cloud denoising networks are trained on datasets with a large number of points like ShapeNet (Chang et al. 2015), so they are not as effective in denoising when applied to sparse upsampled datasets. In particular, the denoising network is more likely to lose sparse details when the noises level is low.

Visual Comparison Experiment

As shown in the Fig 6, we add 1.0% Gaussian noises and compare our network with other networks. We use colors to indicate the magnitude of the error, and our network has a clear advantage over the other networks.

Comparison of coarse output and refined output

To illustrate the specific role of the Position Correction Unit, we perform a visual comparison of the rough point cloud Q' with the refined point cloud Q after the Position Correction Unit. We first add different levels of Gaussian noises to the dataset, and the specific experimental results are shown in Fig 9. We can see from the Fig 9 that the error of the point set is significantly reduced after the Position Correction Unit, which effectively improves the upsampled performance.

Table 6: Comparison with point cloud denoising network. We add different levels of Gaussian noises, simulate the results of scanning with different noises levels using blensor, and compare our method with other methods. We using CD as a quantitative evaluation metric multiplied by 10^{-3} .

method	Noise Robust Test with Gaussian noises						Noise Robust Test with noises by blensor					
	4X			16X			4X			16X		
	0.5%	1.0%	2.0%	0.5%	1.0%	2.0%	0.5%	1.0%	2.0%	0.5%	1.0%	2.0%
DMRDenoise + PU-Net	3.6921	3.4081	2.5479	3.0960	3.0090	2.2145	2.5251	2.6953	2.2278	2.2666	2.1937	1.7936
DMRDenoise + PU-GAN	3.6146	3.6705	2.6507	3.2563	3.1849	2.3677	2.6896	2.9023	2.5874	2.4339	2.5207	2.1199
DMRDenoise + PU-GCN	4.0825	4.1882	2.9777	3.4907	3.6109	2.7163	3.0476	3.2527	3.1554	2.5554	2.7896	2.5704
DMRDenoise + Dis-PU	4.0271	4.3097	3.0841	3.6366	3.8663	2.9202	3.0398	3.3686	3.0828	2.6852	3.0556	2.7149
Ours	0.2792	0.3713	0.7380	0.1422	0.2184	0.5486	0.2854	0.4606	1.4601	0.1110	0.2643	1.1836

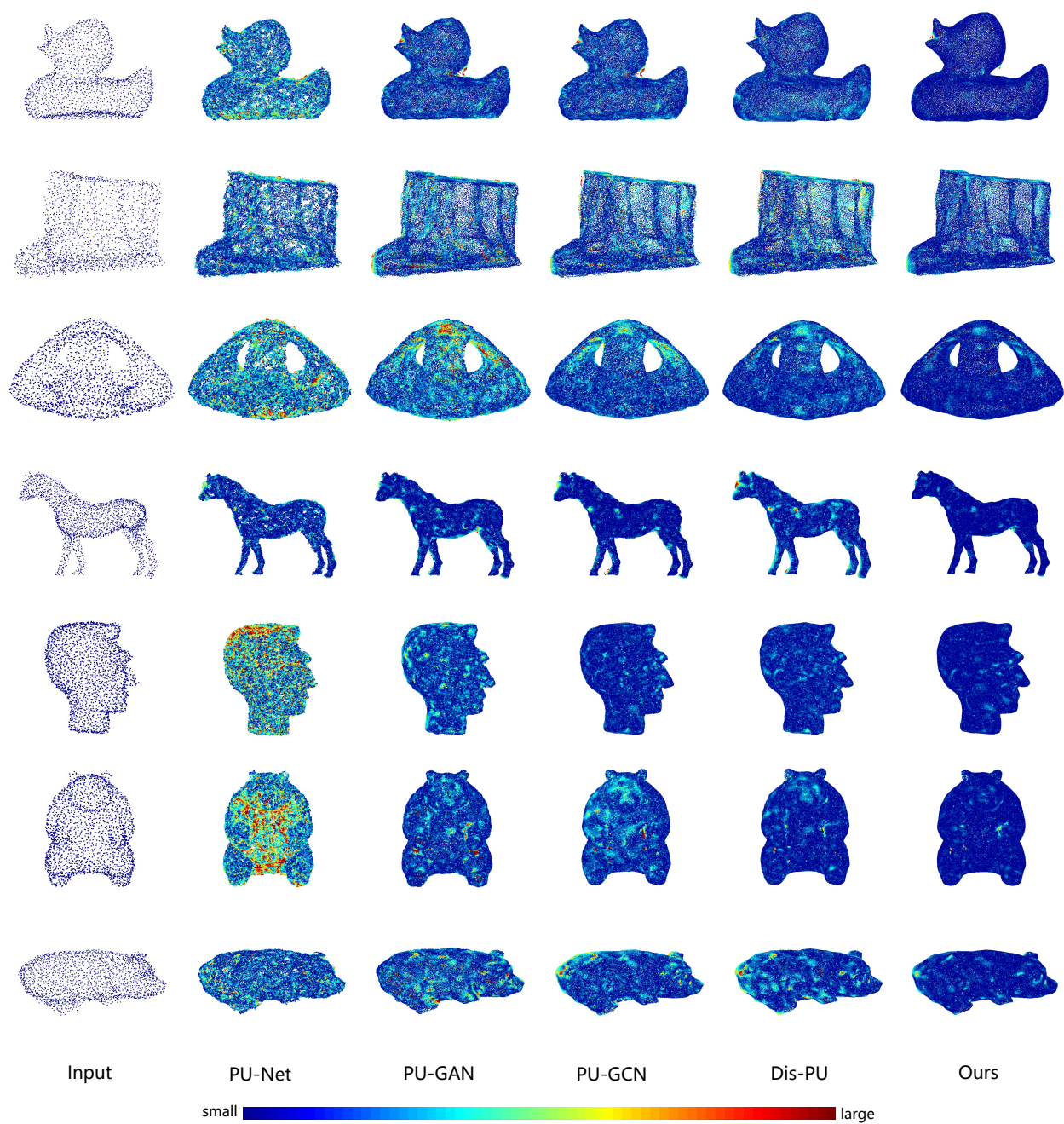


Figure 8: Noises Robust Test with Gaussian noises visual comparison. We use a Gaussian noises of 1.0% as an example to compare our visual effect with other networks. We use color to indicate the CD distance, and the smaller the CD distance, the better the result.

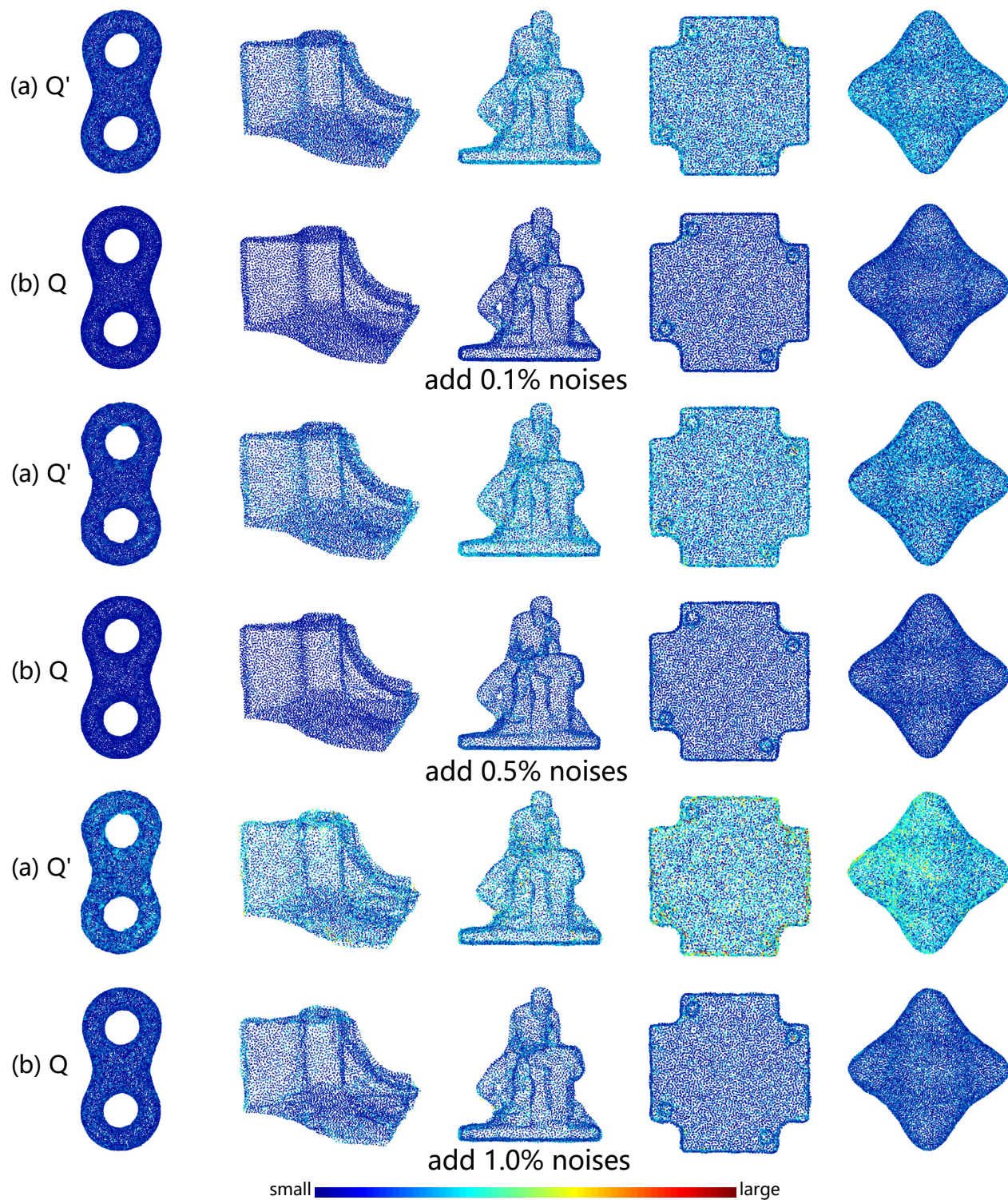


Figure 9: Visualization results for the ablation study. (a) denotes our rough output Q' and (b) denotes the corrected result Q after the Position Correction Unit. We use color to indicate the CD distance, and the smaller the CD distance, the better the result.